JOURNAL OF MATERIALS SCIENCE 26 (1991) 5403–5410

An approach to the mechanical behaviour of SiC/SiC and C/SiC ceramic matrix composites

Part 1 *Experimental results*

E. INGHELS, J. LAMON*
Ecole Nationale Supérieure des Mines, Paris, France

The mechanical behaviour of two woven composites C/SiC and SiC/SiC was investigated at room temperature. The non-linear load–displacement curves and the damaging process were closely related to the specific structure of the composites, consisting of a network of impregnated bundles of fibres. The damage in the bundles proceeded by multiple cracking in the matrix before fibre failure, and dictated the response to the applied load. Other mechanisms, consisting mainly of distortions in bundles and their framework, induced a residual deformation and an energy dissipation. The behaviour was characterized according to the damaging process. Stress–electric strain curves revealed a mechanical response similar to those observed in unidirectional composites, although some effect of the specimen geometry on the curves was observed. Residual strains were similar in tensile and bending conditions. The work of fracture was consistently described by a volumetric rate of energy absorption, related to the applied strain, but the respective contributions of different damage mechanisms could not be determined.

1. Introduction

The introduction of fibres into ceramic matrices is considered a promising way to achieve significant decreases in brittleness, inherent in this class of materials [1, 2]. Based upon the mechanical behaviour, the wide range of ceramic composites presently available can be classified into two categories. The mechanical behaviour usually remains brittle in short fibre-reinforced ceramics, whereas the fracture toughness is improved [2, 3]. Continuous fibres have better efficiency, as they limit the extent of damage in the matrix, and induce non-linear stress–strain relations [4, 5].

Unidirectional composites with continuous fibres (mainly with glass matrix) have been extensively investigated. Multiple cracking was observed in the matrix before fibre failure [4, 6]. A theoretical analysis of this phenomenon and of relations between composite behaviour and fibre and matrix properties has been proposed by Aveston *et al.* [7, 8], and improved by other workers [9, 10]. These approaches predict an increased fracture stress for the matrix. Multidirectional composites with continuous fibres have received less attention. The small amount of experimental data available indicates that they have a mechanical behaviour which is more complex than that of unidirectional composites [11, 12]. The behaviour is either linear or non-linear, depending on the fibre framework. The damaging process depends also on the fibre framework. Basically, delaminations and fibre failures occur both perpendicular to and parallel to the applied stresses. The macroscopic behaviour then results from the combination of the various damaging mechanisms [12, 13].

This paper investigates the mechanical behaviour of two woven composites with a silicon carbide matrix. An experimental study was carried out at room temperature, using various test specimen geometries [14]. We report here the results obtained on the tensile and bending specimens. The proposed analysis of the mechanical behaviour considers separately the contributions of the fibre bundles impregnated by the matrix and of the bundle framework. In Part 2 of the paper, a model of the mechanical behaviour of these composites will be developed, based upon the properties of the fibres and the matrix, and compared with the experimental data of this paper.

2. Experimental procedure

The C/SiC and SiC/SiC composites investigated were provided by the SEP company (Bordeaux, France). They were reinforced by carbon fibres produced by the SEP company, or by silicon carbide fibres ("Nicalon" fibres from the Nippon Carbon Company). These composites are processed in two stages. A bidirectional framework of fibre bundles is first manufactured; the silicon carbide matrix is then deposited on the bundles by a chemical vapour infiltration process at temperatures around 1000 °C.

* *Present address*: Battelle–Geneva, 7, Route de Drize, CH-1227 Carouge, Geneva, Swizerland.

0022–2461/91 $03.00 + .12

The composites are constituted by a stack of identical layers, each consisting of a tissue of impregnated bundles (Fig. 1). Different woven structures are used in the two materials. In the C/SiC composite, the bundles have a smaller diameter, and they are less strongly linked than in the SiC/SiC. Fig. 1 shows the presence of an important porosity, mainly located between the bundles. Therefore, these composites may be regarded as a network of impregnated bundles, rather than continuous materials. The characteristics of the composite constituents are given in Table I. Fibre properties are available in the literature [15, 16]. Since the matrix properties were not available, it was assumed that they can be satisfactorily characterized by the properties of monolithic silicon carbide ceramics.

In the present study, the composites were tested parallel to the layer plane, as they exhibit poor transverse properties. The test specimens contained at least 10 layers of bundles, and one direction of bundles was aligned with the dominant applied tensile stress. Certain SiC/SiC test specimens were also tested with the fibres inclined at 45° to the applied stresses.

TABLE I Properties of fibres and matrix involved in the composites

	C/SiC	SiC/SiC
Fibre		
Radius (μm)	4	7
Elastic modulus (GPa)	180	190
Volumetric fraction	0.28	0.45
Strength (GPa)	0.7–2.5	1.0–2.0
Matrix		
Elastic modulus (GPa)	350	350
Volumetric fraction	0.45–0.65	0.40–0.45
Fracture surface energy ($J\,m^{-2}$)	25	25

The dimensions of the tensile and bending specimens are given in Fig. 2. Various dimensions were used. For tensile specimens, the gauge length varied from 15 to 35 mm. Upper spans of 0, 15 and 30 mm, and various specimen widths were used for the bending tests.

The tests were conducted on an Instron machine, at a constant crosshead speed of 0.2 mm min^{-1}. The applied load P was recorded against the displacement δ. δ was measured between two clips which were stuck to the gauge section of the tensile specimens, and to the tensile surfaces of the bending specimens. The length l between the two clips was similar to the gauge

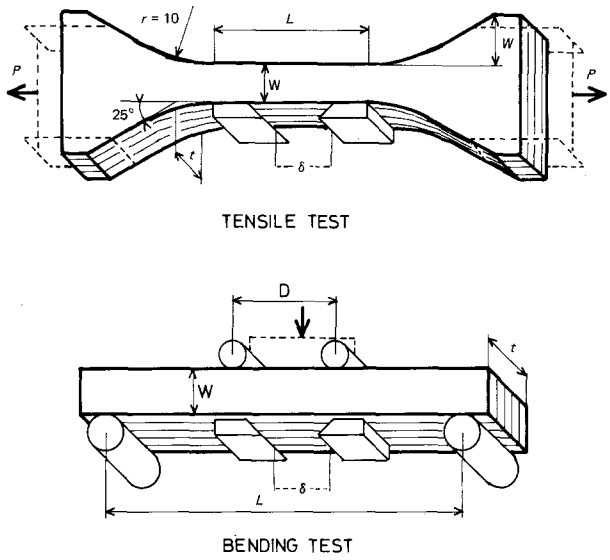

Figure 2 Specimen geometries used in tensile and bending tests.

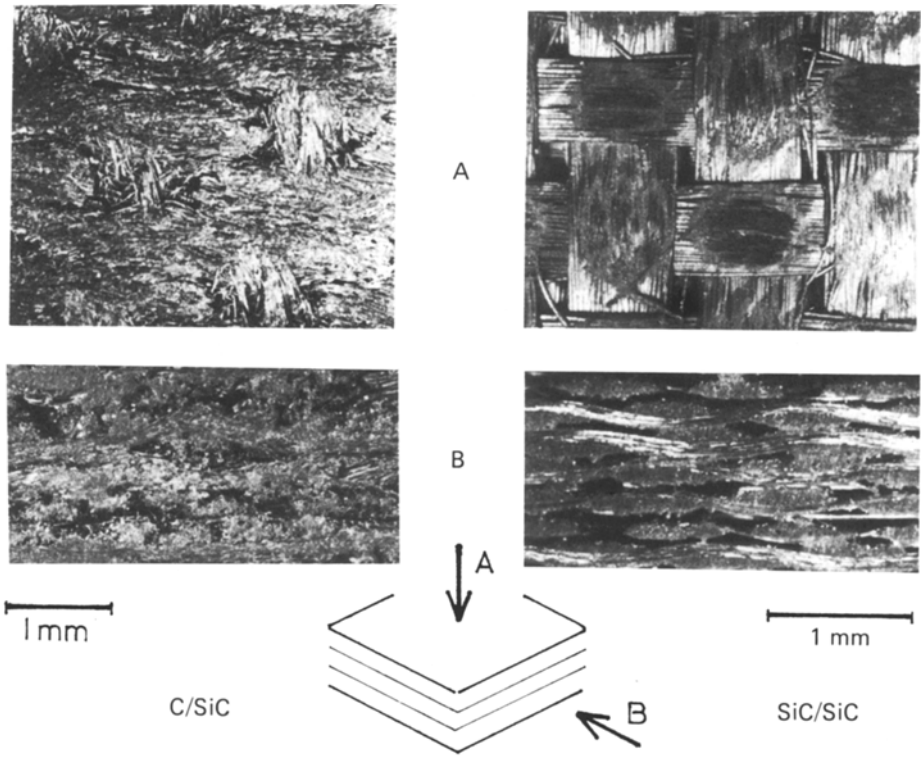

Figure 1 Structure of the as-received materials.

length for the tensile specimens, and around 15 mm for the bending specimens. Each test consisted in a monotonic loading until ultimate specimen fracture. Certain specimens were subjected to repeated partial unloadings. The slopes $\Delta\delta/\Delta P$ of the linear curves obtained on unloading and also on the subsequent loading were similar. They measured the compliance C of the specimen.

3. Mechanical behaviour and damaging process

3.1. Macroscopic behaviour

The typical load–displacement curves which were obtained are shown in Fig. 3. The mechanical behaviour is initially linear elastic. Then, a non-linear region was observed, reflecting matrix damage which induced significant compliance increases, and residual displacements. Finally, fibre failures, initiating at maximum load, caused the unstable fracture of the composites.

As expected with orthotropic materials, the fracture surfaces are perpendicular to the dominant applied stress, and roughly planar. However, detailed investigation revealed that the fracture surfaces were discontinuous, following the network of bundles (Fig. 4). The fractions of bundles involved in the damaging process depend on their orientation to the applied stresses. In a $-45/45$ structure, all the bundles experience similar damage. In the 0/90 structure, the mechanical behaviour is dictated by the bundles parallel to the applied stress. The perpendicular bundles do not contribute significantly to the damaging process.

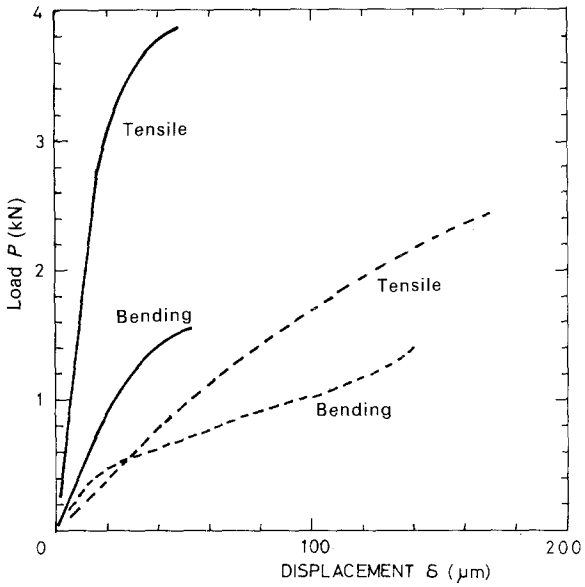

Figure 3 Examples of load–displacement curves measured in the composites. ---, C/SiC; ——, SiC/SiC.

Figure 4 Surface of fracture in the SiC/SiC material.

3.2. Damage mechanisms of the impregnated bundles

The damage mechanisms acting on the impregnated bundles were identified by SEM observation of the fractured surfaces. The examination of specimens which had been previously loaded at various stress levels also allowed the chronology of occurrence of the different mechanisms to be established. All the observed bundles showed the same damage, which didn't seem to be affected by the specimen geometry, the bundle orientation or its location within the specimens. The damage consisted mainly of multiple cracking in the matrix. All the cracks were perpendicular to the fibres (Fig. 5). The distance between successive cracks was roughly constant, between 50 and 100 μm in the C/SiC, and between 20 and 50 μm in the SiC/SiC. Secondary mechanisms were also observed in C/SiC. They include interface debonding, radial cracking and some delaminations in the bundles perpendicular to the applied stresses, occurring early during the loading.

Matrix cracking is then followed by fibre failure, which proceeds first by the successive failures of individual fibres. At each fibre failure, the load is transferred to the neighbouring surviving fibres, promoting

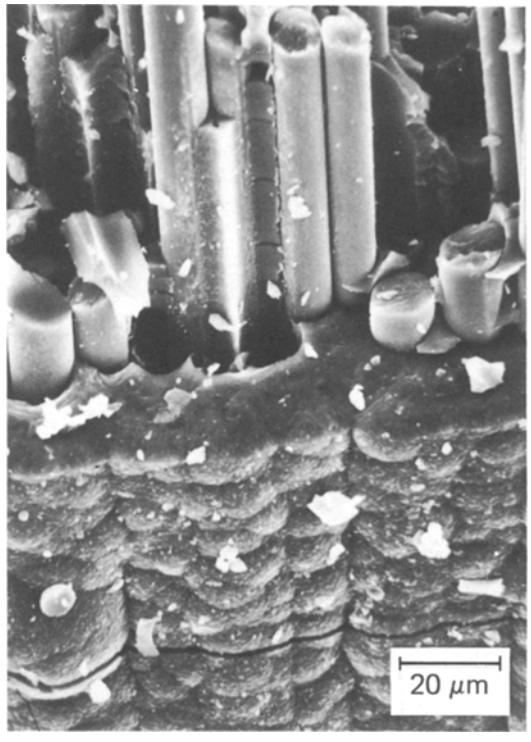

Figure 5 Multiple cracking of the matrix (SiC/SiC material).

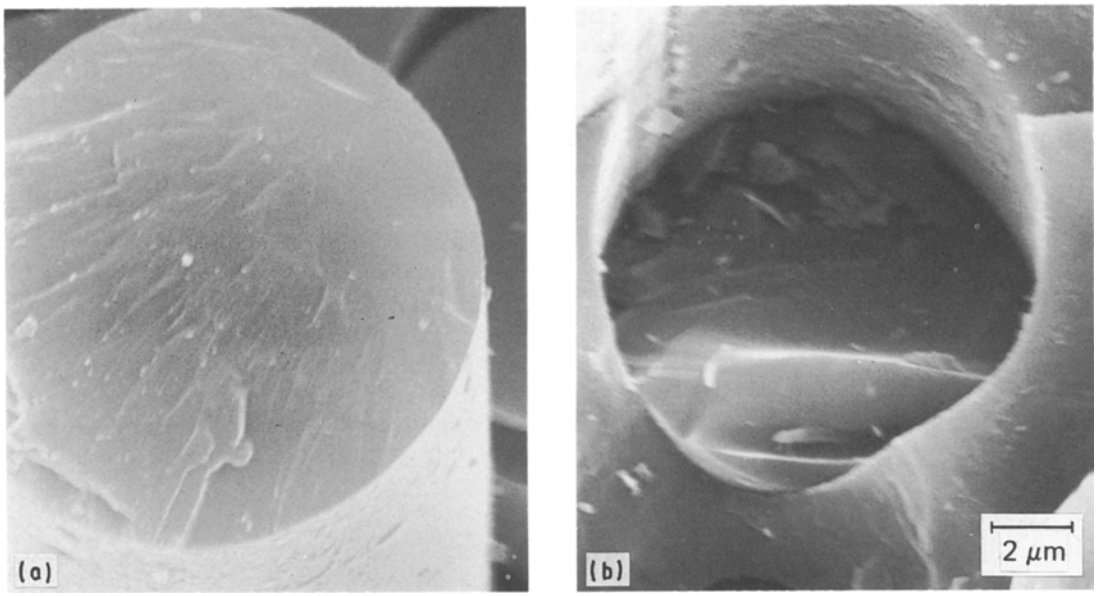

Figure 6 Surfaces of fracture in silicon carbide fibres, (a) with and (b) without a mirror of fracture.

new individual failures. Instability is reached when the remaining fibres cannot carry the applied load. This two-stage process was revealed by the presence of different types of fracture surfaces, which were observed on the fibres, as shown by Fig. 6 for the silicon carbide fibres. Around 30% of the fibres exhibited a fracture mirror, which indicated that failure was initiated by a defect located at the interior of the fibres. These fibres controlled the initial stable stage of fibre failures. The other fibres didn't show any site of fracture initiation, and also exhibited a fracture surface which coincided with the plane of matrix cracking. They broke altogether as failure became unstable.

4. Analysis of mechanical behaviour

4.1. Method

The two composites may be assumed to have the mechanical behaviour of a unidirectional composite consisting of the impregnated bundles, plus some additional residual phenomena, involving the bundles and their framework.

The distortions involving the bundles and the woven network could not be directly observed. However, they are suggested by the presence of residual displacements. The damaging process which first affects the impregnated bundles is usually observed on unidirectional composites having a brittle matrix [4, 7].

For the analysis, the load–displacement curves were divided into two parts reflecting the above-mentioned 'reversible' and 'residual' behaviours. The elastic displacement δ_e and the residual displacement δ_r were derived from the load P, the displacement δ and the compliance C using the following relations:

$$\delta_e = CP \qquad \delta_r = \delta - CP \tag{1}$$

The reversible behaviour, involving the response of impregnated bundles to the applied load, was described by the curve $P(\delta_e)$. The residual behaviour, which was assumed to result from the distortions affecting the materials, was characterized using the plots of δ_r and W_f (W_f is the energy absorbed by the specimen) as a function of δ_e.

Load and displacement were then expressed in terms of stress and strain, calculated in the high-stress regions of specimens where fracture occurred. A stress σ was deduced from the load P, using the relation provided by the theory of linear elasticity. Average strains ε_e and ε_r were derived from the values of the elastic and residual displacements using the following equations (the symbols are described in Figs 7 and 8).

$$\varepsilon_e = \sigma_e/l \quad \varepsilon_r = \sigma_r/l \tag{2}$$

$$\sigma = P/BW \text{ (tensile);}$$

$$\sigma = 1.5PL/(BW^2) \text{ (bending)} \tag{3}$$

The absorbed energy was defined as the difference between the energy stored by the specimen and the elastic energy. The first term was expressed by the area under the load–displacement curve $P(\delta_p)$, where δ_p is the displacement of the loading point. δ_p was related to the measured displacement δ as shown in Figs 7

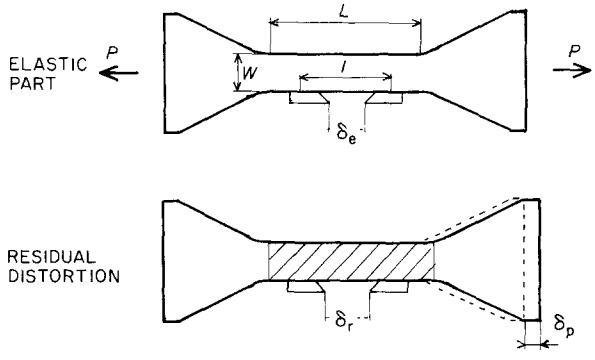

Figure 7 Elastic and residual deformations of a tensile specimen.

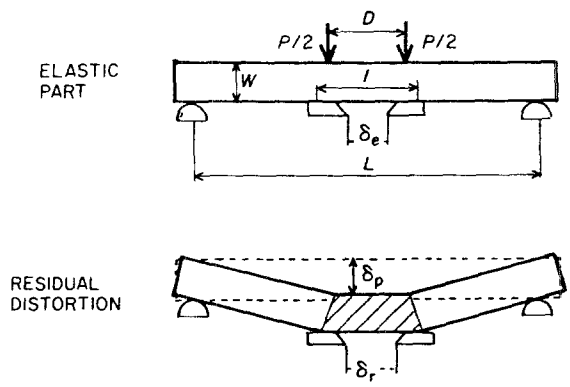

Figure 8 Elastic and residual deformations of a bending specimen.

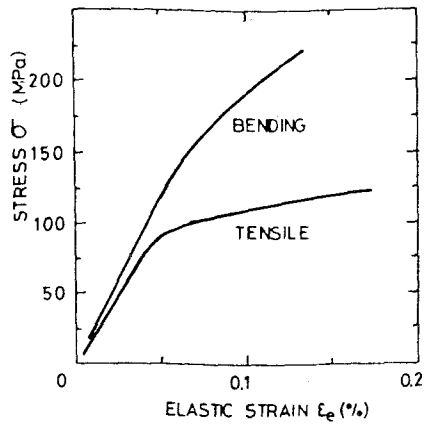

Figure 9 Experimental reversible behaviour (in SiC/SiC material).

and 8, and detailed in the Appendix. The total deformation of specimens was assumed to be the sum of the linear elastic strain distribution, and of a residual strain distribution. The residual strain in tensile specimens was supposed to be uniform over the gauge section. In the bending specimens, the location of residual strain was assumed to be restricted to the region between the upper pins, and to be increasing through the specimen section towards the tensile surface. These residual distributions were found to be consistent with profile measurements performed on damaged specimens [14]. The relations used for calculating the absorbed energy are given in the following equation, with the symbols used in Figs 7 and 8:

$$W_f = \int P\,d\delta - \delta_e P/2 \text{ (tensile)} \quad (4)$$

$$W_f = (L - D)(L + 2D)/(12W) \times \left(\int P\,d(\varepsilon_e + 1.5D\varepsilon_r/(1 + 2D)) - P\varepsilon_e \right) \text{ (bending)}$$

4.2. Reversible behaviour

Examples of reversible behaviour are shown in Fig. 9. The curves $\sigma(\varepsilon_e)$ can be described by two distinct linear parts. The first part characterizes the elastic behaviour and the second one describes the behaviour of the material damaged by matrix cracking. These curves were characterized by the following six parameters, as defined in Fig. 10: the elastic modulus of the undamaged and damaged materials, given by the slopes of each part, the stresses and the elastic strains marking the elastic limit and ultimate fracture.

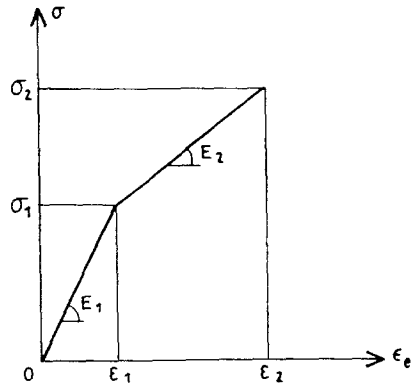

Figure 10 Characterization of the stress–elastic strain curves by six parameters.

As shown by Table II, the results are not significantly altered by dimensions, such as the gauge length of the tensile specimens or the upper span of the bending specimens. However, the test data were affected by testing conditions similarly in both materials. In bending conditions, the non-linearity initiated at higher levels of stress and strain, and the ultimate strength was twice larger than in tensile conditions.

The SiC/SiC appeared stiffer than the C/SiC, although the elastic properties of fibres and matrix were similar in both cases (Table I). The non-linearity thus initiated at stess levels which were close to the ultimate strength σ_2.

TABLE II Experimental data of the parameters used to describe the reversible behaviour (standard deviation)

Parameter	E_1 (GPa)	ε_1 (E – 3)	σ_1 (MPa)	E_2 (GPa)	ε_2 (E – 3)	σ_2 (MPa)
C/SiC (0)						
Tensile	85 (27)	0.7 (0.6)	49 (17)	35 (8)	2.3 (0.9)	83 (11)
Bending	80 (12)	1.1 (0.3)	82 (18)	42 (12)	3.6 (0.6)	175 (17)
SiC/SiC (0)						
Tensile	215 (118)	0.5 (0.2)	83 (27)	64 (22)	1.4 (0.9)	120 (15)
Bending	235 (45)	0.6 (0.2)	137 (21)	125 (14)	1.2 (0.2)	223 (12)
SiC/SiC (45)						
Tensile	276 (108)	0.4 (0.3)	74 (28)	57 (22)	1.1 (0.5)	106 (22)
Bending	272 (33)	0.5 (0.1)	147 (29)	95 (26)	2.0 (0.3)	263 (5)

The above results were not affected by fibre orientation (Table II), which is substantiated by the analogous damaging processes observed on SiC/SiC composites with different fibre orientations to stresses. Fracture was not affected by the shear stresses perpendicular to the fibres, and the damaging process seemed to be mainly dictated by those stresses parallel to the fibres.

4.3. Residual behaviour

Similar $\varepsilon_r(\varepsilon_e)$ and $W_f(\varepsilon_e)$ curves were obtained for both specimen geometries and both materials. Residual displacements and absorbed energies were observed above an elastic strain ε'. Then they increased linearly until the specimen fractured. Experimental curves are shown in Fig. 11. They were described by the threshold ε'_1, the average rates of deformation ($p_\varepsilon = \Delta\varepsilon_r/\Delta\varepsilon_e$) and energy ($p_w = \Delta W_f/\Delta\varepsilon_e$) increases, and the ultimate values of residual strain and absorbed energy, as shown in Fig. 12.

Comparison of the threshold ε'_1 to the elastic limit ε_1 derived from the reversible behaviour (Fig. 13) shows that ε'_1 is smaller than ε_1, suggesting that a damage could occur before alteration of the reversible behaviour curve.

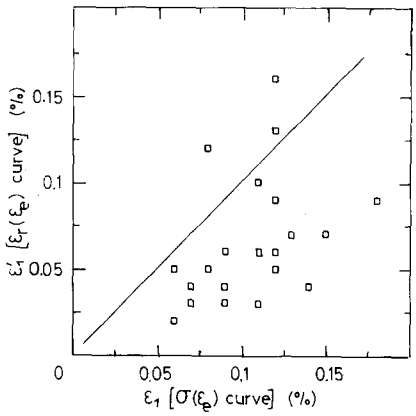

Figure 13 Comparison between the threshold of damage (measured from the residual behaviour) and the non-linearity of the reversible behaviour (matrix cracking).

The experimental residual strain data (Table III) did not exhibit a significant dependence upon the test used. Higher strains were obtained with C/SiC.

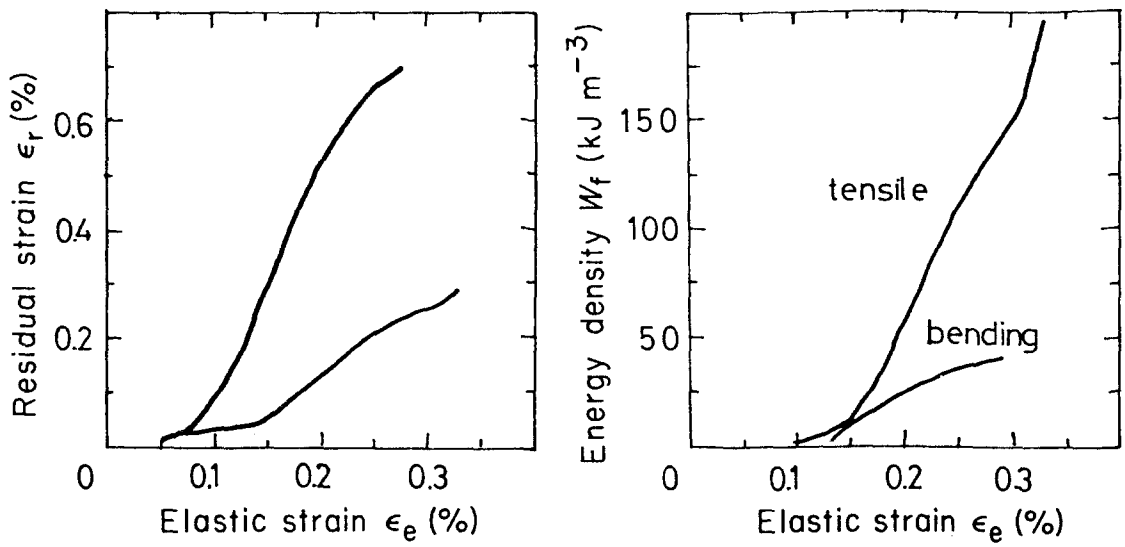

Figure 11 Experimental residual behaviour (in SiC/SiC material).

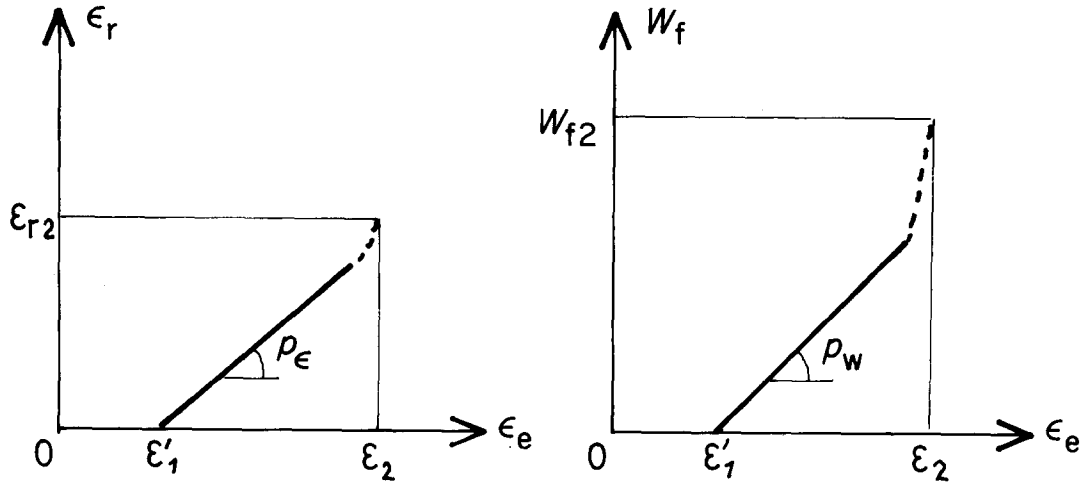

Figure 12 Characterization of the plots $\varepsilon_r(\varepsilon_e)$ and $W_f(\varepsilon_e)$.

TABLE III Experimental data of the parameters used to describe the residual behaviour (standard deviation)

Parameter	p_ε	ε_{r2} $(E-3)$	p_w/vol $(MJ\,m^{-3})$	W_{f2}/surf $(kJ\,m^{-2})$
C/SiC (0)				
Tensile	1.8 (0.6)	2.8 (1.4)	141 (51)	5.2 (2.8)
Bending	3.0 (0.8)	7.6 (2.1)	22 (6)	2.9 (1.1)
SiC/SiC (0)				
Tensile	0.8 (0.6)	1.3 (1.2)	101 (65)	1.8 (1.5)
Bending	–	–	10 (1)	2.3 (2.0)
SiC/SiC (45)				
Tensile	0.4 (0.1)	0.8 (0.6)	76 (37)	2.0 (2.2)
Bending	1.0 (0.3)	1.9 (1.1)	26 (5)	2.1 (1.1)

The absorbed energies are given in Table III. The increase rates p_w were expressed per unit volume, whereas the works of fracture W_{f2} were referred to the cross-section of specimens. This representation was found to be more convenient than comparing specimens with different dimensions. The data obtained on tensile and bending tests cannot be compared as such. Comparison must take into account the strain distributions. The curve $W_f(\varepsilon_e)$ measured in tensile tests provides a constitutive law of energy absorption, since the applied strains are uniform.

In a bending specimen, the absorption of energy in the volume was then evaluated, based on this constitutive law, using the strain distributions described in Fig. 8. The theoretical ratio between the energies measured in bending and in tension was expressed as:

$$W_f[b]/W_f[t] = D/(2L)(1 - (\varepsilon_1'/\varepsilon_2)^2) \quad (5)$$

Equation 5 predicts a ratio of 0.1 to 0.15 for the two composites, which agrees with the experimental data (the scatter of data did not allow the influence of the upper span D to be illustrated). This agreement implies that the values of p_w measured on tensile and bending specimens are satisfactory.

The total energy absorbed during the damaging process is given by the work of fracture W_{f2} (Table III). Values over a range 2 to 4 $kJ\,m^{-2}$ were obtained. However, due to a wide scatter of data, the respective contributions of the progressive absorption related to the strain distribution and described by the parameter p_w, and of the fibre pull-out, could not be separated. The larger work of fracture was observed in the C/SiC, which is consistent with the presence of the higher residual stresses. Moreover, in the SiC/SiC material, fibre orientation did not significantly affect the results.

5. Discussion

The approach based upon the separation of the mechanical behaviour into reversible and residual contributions allowed the complex behaviour of the two composite ceramics to be described using a reduced number of parameters. The differences which were observed between the elastic and ultimate stresses, measured in tensile and bending tests, were comparable to the data which are available for unidirectional composites. In particular, ultimate stresses which were 40% higher in bending than in tension were reported in fibre-reinforced glasses [4, 17]. They were attributed to the non-linear response, which invalidates Equation 3, used for the calculation of stresses in bending tests. No comparison of the data related to the occurrence of matrix cracking and to strains are available in the literature. If it did not result from inaccurate calculations, the effect of the specimen geometry may be related to a volume effect, as usually observed in brittle materials. The differences observed between tensile and bending data are indeed consistent with statistical approaches of fracture, predicting that damage occurs earlier if the stressed volume is more important. Moreover, a statistical aspect was observed in the process of fibre failures. These assumptions will be discussed more extensively in a subsequent paper.

The difference between tensile and bending data did not allow a comparison of experimental results with the predictions from fibre and matrix properties [7]. This comparison could only be made possible for the elastic modulus of the undamaged and damaged materials (parameters E_1 and E_2 in Fig. 10). E_1 was predicted by considering that the materials were laminate composites (0/90), using the laminate theory [19] and the data of Table I. Values of 300 and 270 GPa were obtained for C/SiC and SiC/SiC, respectively. This prediction is consistent with experimental data for SiC/SiC. For C/SiC, the modulus is overestimated to such an extent that this overestimation cannot be attributed to porosity.

For the damaged material, the elastic modulus depends primarily on the stiffness of the fibre framework [7]. The theoretical values of around 40 GPa, which were obtained from Table I, agree with the experimental data (Table II).

The data pertinent to matrix cracking were used to estimate the shear stresses at interfaces. Indeed, the distance l_c between two successive cracks in the matrix, which was found to be roughly constant, is related to the interface strength τ_i by [7]:

$$\tau_i = (r_f V_m E_m)\varepsilon_\mu/(l_c V_f) \quad (6)$$

where ε_μ is the cracking strain of the matrix. Assuming that ε_μ is the non-linearity strain ε_1, interface strengths of 5 and 20 MPa were obtained for C/SiC and SiC/SiC, respectively. Although they are rough estimates, these strengths are consistent with the data determined by the indentation method [19].

Residual strains were expected to involve bundle length increases and some distortions of the woven structure. Bundle length increases were estimated from measurement of crack opening displacements. In the SiC/SiC composites, these estimations were close to the measured residual displacement. In the C/SiC, distortions of the woven structure seemed to be the predominant phenomenon. This difference may be attributed to the woven pattern, which was weaker in the C/SiC composites. The energy absorbing mechanisms could not be identified. Besides the surface energy absorbed by matrix cracking, additional terms probably involve fibre/matrix and bundle/bundle

friction. The respective contributions of the surfaces and frictional terms remain unknown.

6. Conclusion

An experimental study based on tensile and bending tests permitted the identification of the damaging process in two continuous fibre reinforced ceramics (C/SiC and SiC/SiC composites). The analysis of the mechanical behaviour considered separately the reversible behaviour, which is the response of the material to a loading, and the residual behaviour resulting from mechanical damage.

The stress–elastic strain curves consisted of two linear parts, reflecting the main damaging mechanisms. A multiple cracking of the matrix causes a slope change. The second part reflects the deformations of the damaged material. The ultimate stress shows the fibre failures. Both the damaging process and the behaviour curve are similar to those pertinent to a unidirectional composite containing a brittle matrix.

The extent of the damage was characterized by the measured residual displacements and by the energy absorbed before fracture. Both are related to matrix cracking and to various frictional phenomena within the material, occurring at fibre/matrix interfaces or between the bundles. They depend mainly on the woven structure. The magnitude of residual displacements differentiates both composites, but also composites and monolithic ceramics. High residual strains caused a dramatic increase in the work of fracture, which was much more important than in brittle ceramics.

However, further studies are still required to achieve a sound characterization of these materials. The simplified calculation of the reversible curve induced discrepancies between the data obtained in tensile and in bending conditions. Therefore, this curve cannot be considered as a characteristic of the material until further analysis is conducted. The extent of the damage was roughly estimated. In particular, it does not allow an estimation of the respective contributions of damaging mechanisms. These questions will be examined in a subsequent paper, by a behaviour model and a simulation of the load–displacement curve for various specimen geometries.

Acknowledgements

This work was supported by DRET under contracts nos 82305 and 84082.

Appendix: Derivation of the displacement at the loading line from the measured displacement

In tensile specimens, δ involved the whole gauge section, and the design of the specimen allowed the deformation of the part located between the loading point and the gauge section to be neglected. Then the displacement δ_p was assumed equal to δ.

In bending specimens, the elastic part of δ_p was deduced from δ_e assuming a linear elastic distribution of strains

$$\delta_{pe} = (L - D)(L + 2D)\varepsilon_e/W/6 \qquad \text{(A1)}$$

The residual part was obtained from the model of specimen deformation described in Fig. 8. Between the upper pins, the residual strain is equal to 0 and ε_r, respectively, on the compressive and tensile surfaces. Then, an angular distortion $\alpha = (\varepsilon_r D)/(2W)$ of the cross-section induces a rotation of each remaining half-arm of the beam. The resulting displacement at the loading point is

$$\begin{aligned}\delta_{pr} &= (L - D)\alpha/2 \\ &= (L - D)D\varepsilon_r/W/4 \qquad \text{(A2)}\end{aligned}$$

and then, by adding (A1) to (A2)

$$\begin{aligned}\delta_p = {} & (L - D)(L + 2D) \\ & \times [\varepsilon_e + 1.5D\varepsilon_r/(L + 2D)]/W/6 \qquad \text{(A3)}\end{aligned}$$

References

1. R. W. RICE, *Ceram. Eng. Sci. Proc.* **2** (1981) 661.
2. I. W. DONALD and P. W. McMILLAN, *J. Mater. Sci.* **11** (1976) 949.
3. V. LAWS, *J. Phys. D: Appl. Phys.* **4** (1971) 1737.
4. D. B. MARSHALL and A. G. EVANS, *J. Amer. Ceram. Soc.* **68** (1985) 225.
5. K. M. PREWO, J. J. BRENNAN and G. K. LAYDEN, *Amer. Ceram. Soc. Bull.* **65** (1986) 305.
6. K. M. PREWO and J. J. BRENNAN, *J. Mater. Sci.* **15** (1980) 463.
7. J. AVESTON, G. A. COOPER and A. KELLY, in "Properties of Fibre Composites" (IPC, Guildford, 1971) p. 15.
8. J. AVESTON and A. KELLY, *J. Mater. Sci.* **8** (1973) 352.
9. B. BUDIANSKY, J. W. HUTCHINSON and A. G. EVANS, *J. Mech. Phys. Solids* **34** (1986) 167.
10. J. G. MORLEY, *J. Mater. Sci.* **18** (1983) 1564.
11. M. R'MILI, R. ROUBY and R. POINT, *Proc. JNC5, eds Pluralis, Paris*, Sept. (1986) 299.
12. O. SBAIZERO and A. G. EVANS, *J. Amer. Ceram. Soc.* **69** (1986) 481.
13. P. LADEVEZE, *Proc. JNC5, edn Pluralis, Paris*, Sept (1986) 667.
14. E. INGHELS, PhD thesis, Ecole Nationale Supérieure des Mines de Paris (1987).
15. J. L. C. DA SILVA and D. J. JOHNSON, *J. Mater. Sci.* **19** (1984) 3201.
16. G. SIMON and A. R. BUNSELL, *ibid.* **19** (1984) 3649.
17. V. LAWS, *ibid.* **16** (1981) 1299.
18. S. W. TSAI and H. T. HAHN, "Introduction to Composite Materials" (Editions Technomic, 1980).
19. J. JAMET, "Les composites a matrice fragile, leur mécanique de la rupture, leur élaboration via les organométalliques" (Technical Report 7/3548M, ONERA, September 1983).

Received 28 November 1988
and accepted 8 May 1989